

1 **Revisiting the Steering Principal of Tropical Cyclone Motion in a Numerical**
2 **Experiment**

3
4
5 Liguang Wu^{1,2} and Xiaoyu Chen¹

6 ¹Key Laboratory of Meteorological Disaster, Ministry of Education (KLME), Pacific
7 Typhoon Research Center (PTRC), Nanjing University of Information Science &
8 Technology, Nanjing, China

9 ²State Key Laboratory of Severe Weather, Chinese Academy of Meteorological
10 Sciences, Beijing, China

11
12
13
14
15
16
17 Nov. 14, 2016

18
19 Revised for *Atmospheric Chemistry and Physics*

20
21
22
23 Corresponding author address: Prof. Liguang Wu
24 Pacific Typhoon Research Center
25 Nanjing University of Information Science and Technology, Nanjing, Jiangsu 210044,
26 China
27 E-mail: liguang@nuist.edu.cn

Abstract

30

31 The steering principle of tropical cyclone motion has been applied to tropical
32 cyclone forecast and research for nearly 100 years. Two fundamental questions
33 remain unanswered. One is why the steering flow plays a dominant role in tropical
34 cyclone motion and the other is when tropical cyclone motion deviates considerably
35 from the steering. A high-resolution numerical experiment was conducted with the
36 tropical cyclone in a typical large-scale monsoon trough over the western North
37 Pacific. The simulated tropical cyclone experiences two eyewall replacement
38 processes.

39 Based on the potential vorticity tendency (PVT) diagnostics, this study
40 demonstrates that the conventional steering, which is calculated over a certain radius
41 from the tropical cyclone center in the horizontal and a deep pressure layer in the
42 vertical, plays a dominant role in tropical cyclone motion since the contributions from
43 other processes are largely cancelled out due to the coherent structure of tropical
44 cyclone circulation. Resulting from the asymmetric dynamics of the tropical cyclone
45 inner core, the trochoidal motion around the mean tropical cyclone track cannot be
46 accounted for by the conventional steering. The instantaneous tropical cyclone motion
47 can considerably deviate from the conventional steering that approximately accounts
48 for the combined effect of the contribution of the advection of the symmetric potential
49 vorticity component by the asymmetric flow and the contribution from the advection
50 of the wavenumber-one potential vorticity component by the symmetric flow.

51

52 **1. Introduction**

53 The environmental steering principle has been applied to tropical cyclone track
54 forecasting for nearly 100 years (Fujiwara and Sekiguchi 1919; Bowie 1922), which
55 states that a tropical cyclone tends to follow the large-scale flow in which it is
56 embedded. Such a steering concept has been extended to include the beta drift (also
57 called secondary steering) that arises mainly from the interaction between tropical
58 cyclone circulation and the planetary vorticity gradient (Holland 1983; Chan 1984;
59 Chan and Williams 1987; Fiorino and Elsberry 1989; Carr and Elsberry 1990; Wang
60 and Li 1992; Wang and Holland 1996a). The steering flow is usually calculated over a
61 certain radius from the tropical cyclone center in the horizontal and a deep pressure
62 layer in the vertical (Dong and Neumann 1986; Velden and Leslie 1991; Franklin et al.
63 1996). For convenience, here we call it the conventional steering flow. As a rule of
64 thumb, the conventional steering flow has been extensively used in tropical cyclone
65 track forecasting and understanding of tropical cyclone motion (e.g., Simpson 1948;
66 Riehl and Burgner 1950; Chan and Gray 1982; Fiorino and Elsberry 1989; Neumann
67 1993; Wu and Emanuel 1995a, b; Wang and Holland 1996b, c; Wu et al. 2011a; Wu et
68 al. 2011b). Given complicated interactions between tropical cyclone circulation and
69 its environment, tropical cyclone motion should not be like a leaf being steered only
70 by the currents in the stream. Therefore, two fundamental issues are still remaining on
71 the steering principle. First, why can the conventional steering play a dominant role in
72 tropical cyclone motion? Second, when may tropical cyclone motion deviate
73 considerably from the conventional steering?

74 The potential vorticity tendency (PVT) paradigm for tropical cyclone motion was
75 proposed by Wu and Wang (2000), in which a tropical cyclone tends to move to the
76 region of the PVT maximum. In other words, tropical cyclone motion is completely
77 determined by the azimuthal wavenumber-one component of PVT and all of the
78 factors that contribute to the azimuthal wavenumber-one component of PVT play a
79 potential role in tropical cyclone motion. The contributions of individual factors can
80 be quantified through the PVT diagnosis and the steering effect is one of the factors
81 (Wu and Wang 2000). Wu and Wang (2000, 2001a) evaluated the PVT approach using
82 the output of idealized numerical experiments with a coarse spacing of 25 km and
83 understood the vertical coupling of tropical cyclone circulation under the influence of
84 vertical wind shear. Wu and Wang (2001b) found that convective heating can affect
85 tropical cyclone motion by the heating-induced flow and the positive PVT that is
86 directly generated by convective heating.

87 The PVT paradigm was further verified by Chan et al. (2002). The observational
88 analysis indicated that the potential vorticity advection process is generally dominant
89 in tropical cyclone motion without much change in direction or speed while the
90 contribution by diabatic heating is usually less important. An interesting finding of the
91 study is that the contribution of diabatic heating becomes important for irregular
92 tropical cyclone motion, suggesting that track oscillations as well as irregular track
93 changes may be explained by changes in the convection pattern. The PVT approach
94 has been used in understanding tropical cyclone motion in the presence of the effects
95 of land surface friction, river deltas, coastal lines, mountains, islands, cloud-radiative

96 processes and sea surface pressure gradients (e.g., Wong and Chan 2006; Yu et al.
97 2007; Fovell et al. 2010; Hsu et al. 2013; Wang et al. 2013; Choi et al. 2013).

98 As we know, the coarse resolution of the numerical experiment in Wu and Wang
99 (2000) was unable to resolve the eyewall structure and tropical cyclone rainbands,
100 which may affect tropical cyclone motion (Holland and Lander 1993; Nolan et al.
101 2001; Oda et al. 2006; Hong and Chang 2009). Under the PVT paradigm, in this study
102 we use the output from a high-resolution numerical experiment to address the
103 aforementioned two fundamental issues that are important to understanding tropical
104 cyclone motion. The numerical experiment was conducted with the advanced research
105 version of the Weather Research and Forecast (ARW-WRF) model. In particular, an
106 initially symmetric baroclinic vortex is embedded in the low-frequency atmospheric
107 circulation of Typhoon Matsa (2005) to simulate tropical cyclone motion in a realistic
108 large-scale environment. For simplicity, the present study focuses on the numerical
109 experiment without the influences of land surface and topography.

110 **2. The output of the numerical experiment**

111 The numerical experiment conducted with the WRF model (version 2.2) in this
112 study contains a coarsest domain centered at 30.0°N, 132.5°E and four two-way
113 interactive domains. In order to better simulate the tropical cyclone rainbands and
114 eyewall structure, the horizontal resolutions are 27, 9, 3, 1, 1/3 km, respectively. The
115 three innermost domains move with the tropical cyclone (Fig. 1). The model consists
116 of 40 vertical levels with a top at 50 hPa. The WRF single-moment 3-class scheme
117 and the Kain-Fritsch cumulus parameterization scheme (Kain and Fritsch 1993) are

118 used in the outermost domain. The WRF single-moment 6-class scheme (Hong and
119 Lim 2006) and no cumulus parameterization scheme are used in the four inner
120 domains. The other model physics options are the Rapid Radiative Transfer Model
121 (RRTM) longwave radiation scheme (Mlaewe et al. 1997), the Dudhia shortwave
122 radiation scheme (Dudhia 1989), and the Yonsei University scheme for planetary
123 boundary layer parameterization (Noh et al. 2003).

124 The National Centers for Environmental Prediction (NCEP) Final (FNL)
125 Operational Global Analysis data with resolution of $1.0^\circ \times 1.0^\circ$ at every 6 h were used
126 for deriving the large-scale background with a 20-day low-pass Lanczos filter
127 (Duchon 1979). The low-frequency fields were taken from those of Typhoon Matsa
128 (2005) from 0000 UTC 5 August to 0000 UTC 9 August 2005. At 0000 UTC 5 August,
129 the typhoon was located to the northeast of Taiwan Island with the maximum surface
130 wind of 45 m s^{-1} . During the following three days, Matsa moved northwestward in the
131 monsoon trough and made landfall on mainland China at 1940 UTC 5 August. The
132 sea surface temperature is spatially uniform being 29°C . The analysis nudging for the
133 wind components above the lower boundary layer is used in the coarsest domain to
134 maintain the large-scale patterns with a nudging coefficient of $1.5 \times 10^{-4} \text{ s}^{-1}$.

135 A symmetric vortex is initially embedded at 25.4°N , 123.0°E (Matsa's center) in
136 the background (Fig. 1). The vortex was spun up for 18 hours on an f-plane without
137 environmental flows to make it relatively consistent with the WRF model dynamics
138 and physics. Considering several hours of the initial spin-up, here we focus only on
139 the 72-hour period from 6 h to 78 h with the output at one-hour intervals. The

140 simulated tropical cyclone takes a northwest north track (Fig. 1), generally similar to
141 that of Typhoon Matsa (2005). The evolution of tropical cyclone intensity is shown in
142 Figure 2. Although the sea level minimum pressure generally decreases with time, the
143 maximum wind speed shows considerable fluctuations.

144 Figure 3 shows the simulated wind and radar reflectivity fields at 700 hPa. The
145 vertical wind shear, which is calculated between 200 hPa and 850 hPa over a radius of
146 500 km from the tropical cyclone center, is also plotted in the figure. The tropical
147 cyclone center is defined as the geometric center of the circle on which the azimuthal
148 mean tangential wind speed reaches a maximum (Wu et al. 2006). We use a
149 variational method to determine the tropical cyclone center each hour at each level.
150 Different definitions of the tropical cyclone center are also used and it is found that
151 fluctuations in tropical cyclone translation do not depend on the specific definition of
152 the tropical cyclone center. At 24 h (Fig. 3a), the vertical wind shear is more than 10
153 m s^{-1} . The eyewall is open to the southwest and strong eyewall convection occurs
154 mainly on the downshear left side (Frank and Ritchie 2001). The rainbands simulated
155 in the innermost domain exhibit apparent cellular structures (Houze 2010), mostly on
156 the eastern side. The eyewall replacement cycle (ERC), which is important for
157 tropical cyclone intensity change (Wu et al. 2012; Huang et al. 2012), is simulated in
158 this numerical experiment. At 48 h (Fig. 3b), the vertical wind shear is weaker and the
159 tropical cyclone undergoes an ERC. At 72 h (Fig. 3c), the outer eyewall just forms
160 while the inner one is breaking during the second ERC. Figure 3 suggests that the
161 simulated tropical cyclone has a structure similar to a typical observed one, especially

162 in the inner core region.

163 Two eyewall replacement processes, which may affect tropical cyclone motion
164 (Oda et al. 2006; Hong and Chang 2009), can be further shown in Figure 4. The
165 evolution of the azimuthal mean component of the 700-hPa wind in the 9-km domain
166 indicates the eyewall replacement processes around 42 h and 68 h, respectively.
167 During the first eyewall replacement, for example, the wind starts to intensify outside
168 the eyewall around 36 h, in agreement with previous numerical studies (Wu et al.
169 2012; Huang et al. 2012). The radius of maximum wind is located at about 40 km
170 after the 6-h spin-up and decreases to about 30 km at 42 h. The lifetime maximum
171 wind speed occurs at 60 h after the second eyewall replacement process (Fig. 2b). We
172 also conducted a similar sensitivity experiment without the sub-kilometer domain.
173 The tropical cyclone track in the experiment is generally similar to that in the
174 sub-kilometer simulation, but no eyewall replacement cycle can be observed in the
175 sensitivity experiment.

176 **3. Dominant role of the conventional steering**

177 The relationship between PVT and tropical cyclone motion can be written as (Wu
178 and Wang 2000)

$$179 \quad \left(\frac{\partial P_1}{\partial t}\right)_f = \left(\frac{\partial P_1}{\partial t}\right)_m - \mathbf{C} \cdot \nabla P_s, \quad (1)$$

180 Where subscripts m and f indicate, respectively, the moving and fixed reference frames
181 and \mathbf{C} is the velocity of the reference frame that moves with the tropical cyclone. In
182 other words, \mathbf{C} is the velocity of tropical cyclone motion, which can vary in the
183 vertical. P_l and P_s are the azimuthal wavenumber-one and symmetric components of

184 potential vorticity with respect to the storm center. It can be seen that the PVT
 185 generated in the fixed reference frame (the term on the left hand side) is provided for
 186 the development of the wavenumber one component (the first term on the right hand
 187 side) and for tropical cyclone motion (the second term on the right hand side). The
 188 first term on the right hand side of Eq. (1) was neglected in Wu and Wang (2000), but
 189 we retain it in this study. The term can be calculated with the two-hour change of the
 190 wavenumber one component in the frame that moves with the tropical cyclone center.

191 The PVT generated in the fixed reference frame can be calculated with the PVT
 192 equation in p -coordinates as

$$193 \quad \frac{\partial P}{\partial t} = -\mathbf{V} \cdot \nabla P - \omega \frac{\partial P}{\partial p} - g \nabla_3 \cdot \left(-\frac{Q}{c_p \pi} \mathbf{q} + \nabla \theta \times \mathbf{F} \right), \quad (2)$$

194 Where P , \mathbf{V} and $\boldsymbol{\omega}$ are potential vorticity, horizontal and vertical components of the
 195 wind velocity, respectively. Eq. (2) contains horizontal advection (HA), vertical
 196 advection (VA), diabatic heating (DH) and friction (FR) terms on the right hand side.

197 Q , θ , \mathbf{q} and \mathbf{F} are diabatic heating rate, potential temperature, absolute vorticity and
 198 friction, while g , c_p and π are the gravitational acceleration, the specific heat of dry air
 199 at constant pressure and the Exner function. ∇_3 and ∇ denote the three and two
 200 dimensional gradient operators.

201 Following Wu and Wang (2000), a least square method is used to estimate the
 202 velocity of tropical cyclone motion (\mathbf{C}) in Eq. (1). The translation velocity is also
 203 calculated with the hourly positions of the tropical cyclone center. For convenience,
 204 the tropical cyclone motion estimated with the PVT diagnostic approach and with the
 205 center position is referred to as the PVT velocity and the tropical cyclone velocity,

206 respectively, in the following discussion. In the PVT approach, we find that the
207 estimated tropical cyclone motion is not much sensitive to the size of the calculation
208 domain. As we know, however, determination of the conventional steering flow for a
209 given tropical cyclone is not unique and depends on the size of the calculation domain
210 (Wang et al. 1998). Here we select the calculation domain to minimize the difference
211 between the tropical cyclone speed and the conventional steering flow. After a series
212 of tests, we find that such a minimum can be reached when the 270-km radius is used.
213 This is consistent with the analysis of the airborne Doppler radar data in Marks et al.
214 (1992) and Franklin et al. (1996). The analysis indicated that tropical cyclone motion
215 was best correlated with the depth-mean flow averaged over the inner region within 3°
216 latitudes. Note that the PVT, tropical cyclone and steering velocities are calculated at
217 each level and then the depth-mean ones are averaged over the layer between 850-300
218 hPa.

219 Figure 5a shows the time series of the magnitudes of the tropical cyclone velocity
220 (black), the PVT velocity (blue) and the conventional steering (red). Note that the
221 PVT velocity and the conventional steering are instantaneous, whereas the tropical
222 cyclone velocity is calculated based on the two-hour difference of the center position.
223 For consistence, a three-point running mean is applied to the PVT speed and the
224 conventional steering. These magnitudes generally increase as the tropical cyclone
225 takes a northwest north track. The mean speeds calculated from the PVT approach
226 and the center positions are 2.86 m s^{-1} and 2.75 m s^{-1} over the 72-h period. Compared

227 to the tropical cyclone speed, the root-mean-square error (RMSE) of the PVT speed is
228 0.22 m s^{-1} , only accounting for 8% of the tropical cyclone speed.

229 Figures 5b and 5c further display the zonal and meridional components of the
230 tropical cyclone velocity (black), the PVT velocity (blue) and the conventional
231 steering (red). While the westward component fluctuates about the mean zonal
232 tropical cyclone (PVT) speed of -1.0 m s^{-1} , the northward component generally
233 increases with time. Figure 5 clearly indicates that the translation velocity of the
234 tropical cyclone can be well estimated with the PVT approach.

235 The environmental and secondary steering flows are indistinctly referred to the
236 conventional steering flow in this study. The conventional steering shown in Fig. 5 is
237 averaged over the same radius (270 km) and the 850-300 hPa layer, as used in the
238 calculation of the PVT speed. The 72-h mean magnitudes of the tropical cyclone
239 velocity and the conventional steering are 2.86 m s^{-1} and 2.87 m s^{-1} , respectively, only
240 with a difference of 6.7° in the motion direction. We also calculated the
241 root-mean-square-error (RMSE) of the conventional steering averaged over various
242 time periods with the tropical cyclone speed (Fig. 6). The RMSE of the magnitude
243 decreases with the increasing average period, generally less than 9% of the translation
244 speed of the tropical cyclone. The difference in direction also decreases with the
245 increasing average period within 9-11 degrees. Considering uncertainties in
246 determining tropical cyclone centers and calculating the steering, we conclude that the
247 conventional steering plays a dominant role in tropical cyclone motion. However,
248 Figure 5 indicates that the instantaneous tropical cyclone motion can considerably

249 derivate from the conventional steering. The conventional steering cannot account for
250 the fluctuations in tropical cyclone motion, which will be further discussed in Section
251 5.

252 **4. Contributions of individual processes**

253 The individual contributions of various terms in the PVT equation to tropical
254 cyclone motion can also be estimated with Eq. (1), as shown by Wu and Wang (2000).
255 In this study, the contribution of the friction (FR) term is calculated as the residual of
256 the PVT equation. Figure 7 shows the individual contributions of the terms in the
257 PVT equation to tropical cyclone motion. While the contribution of the HA term plays
258 a dominant role (Fig. 7c), the figure exhibits considerable fluctuations, suggesting that
259 the contributions of the DH and VA terms tend to cancel each other (Figs. 7a and 7b).
260 Here we discuss the contribution of each term in the PVT equation to understand the
261 dominant role of the conventional steering in tropical cyclone motion.

262 **a. Horizontal advection**

263 As discussed in Wu and Wang (2001b), the HA term in the PVT equation can be
264 approximately written as: $-\mathbf{V}_1 \cdot \nabla \mathbf{P}_s - \mathbf{V}_s \cdot \nabla \mathbf{P}_1$, where \mathbf{V}_s is the symmetric
265 component of the tangential wind and \mathbf{V}_1 is the wavenumber-one component of the
266 asymmetric wind. The first term (HA1) represents the advection of the symmetric
267 potential vorticity component by the asymmetric flow. The second term is the
268 advection of the wavenumber-one potential vorticity component by the symmetric
269 flow (HA2).

270 The contribution of the HA1 term is literally the steering effect, but it is not the
271 conventional steering that is calculated as the velocity of the mean wind averaged
272 over 300-850 hPa within the radius of 270 km from the tropical cyclone center in this
273 study. Wu and Wang (2001a) pointed out that the steering effect in the HA1 term is
274 associated also with the gradient of the symmetric potential vorticity component,
275 which make its contribution be confined to the inner region of tropical cyclones.

276 Figure 8 shows the contributions of the HA1 and HA2 terms, which exhibit
277 considerable fluctuations with time. The contribution of HA and the conventional
278 steering are also plotted. For clarity, the conventional steering is removed from the
279 contribution of HA1 (i.e. HA1'). The 72-hour mean difference between the
280 contribution of HA1 and the conventional steering is -1.25 m s^{-1} in the zonal
281 component and 1.62 m s^{-1} in the meridional component, suggesting that the
282 contribution of the HA1 term is considerably different from the conventional steering.
283 In fact, the contributions of the HA1 and HA2 terms are highly anticorrelated. The
284 correlations for the zonal and meridional components are -0.82 and -0.80 , respectively.
285 The negative correlations suggest the cancellation between the contributions of the
286 HA1 and HA2 terms. As a result, the combined effect of the HA1 and HA2 terms can
287 actually account for the effect of the conventional steering except the short-time
288 fluctuations, as shown in Fig. 8. It is interesting to note that the contributions of the
289 HA1 and HA2 terms increase in magnitude during the two eyewall replacement
290 processes around 42 h and 68 h, suggesting that the tropical cyclone motion
291 considerably deviates from the steering of the asymmetric flow during eyewall

292 replacement. However, it seems that the two eyewall replacement processes have little
293 influence on the tropical cyclone motion (Fig. 5a).

294 The cancellation between the contributions of the HA1 and HA2 terms arises
295 from the interaction between the symmetric and wavenumber-one components of the
296 tropical cyclone circulation. As an example, Figure 9a shows HA1 and the
297 wavenumber-one components of potential vorticity (contours) and winds at 700 hPa
298 after 18 hours of the integration. The positive (negative) anomalies of potential
299 vorticity are nearly collocated with the cyclonic (anticyclonic) circulation. Since the
300 potential vorticity in the inner core is generally elevated, the advection of the
301 symmetric potential vorticity component by the flows between the cyclonic and
302 anticyclonic circulations leads to the maximum (minimum) HA1 in the exit (entrance)
303 of the flows between the cyclonic and anticyclonic circulation. On the other hand, the
304 advection of the wavenumber-one component of potential vorticity by the symmetric
305 cyclonic flow leads to the maximum HA2 in the entrance and the minimum HA1 in
306 the exit (Fig. 9b). Although the contributions of the HA1 and HA2 terms can fluctuate
307 with a magnitude of about 4 m s^{-1} (Fig. 8), their combined effect shows only
308 small-amplitude fluctuations in the tropical cyclone motion. The short-time
309 fluctuations will be discussed in the next section.

310 **b. Contributions of diabatic heating and vertical advection**

311 Some individual contributions in Figs. 7a and 7b are statistically correlated. For
312 example, the zonal contribution of the HA term is negatively correlated with that of
313 the DH term with a coefficient of -0.44, and the meridional contribution of the HA

314 term is negatively correlated with that of the VA terms with a coefficient of -0.54.
315 The correlation coefficients pass the significance test at the 95% confidence level. It is
316 suggested that the contributions of individual terms can partially cancel each other
317 due to the coherent structure of the tropical cyclone.

318 We first discuss the contribution of the VA term. The VA contains two primary
319 terms: the advection of the symmetric component of potential vorticity by the
320 wavenumber-one component of vertical motion (VA1) and wavenumber-one
321 component of potential vorticity by the symmetric component of vertical motion
322 (VA2). Our examination indicates that the contribution of the VA term is dominated
323 by that of VA1. That is, the direction of the contribution of the VA term is determined
324 by the orientation of the wavenumber-one component of vertical motion. Figure 10
325 shows the wavenumber-one components of the 500-hPa vertical motion, 700-hPa
326 winds relative to tropical cyclone motion, and 500-hPa heating rate after 18 hours of
327 integration. We can see that the upward (downward) motion generally occurs in the
328 entrance (exit) region of the 700-hPa winds. Bender (1997) found that vorticity
329 stretching and compression is closely associated with the vorticity advection due to
330 the relative flow (difference between the wavenumber-one flow and the TC motion),
331 but Riemer (2016) recently argued that Bender's mechanism did not work in his
332 idealized experiment. We find that the contribution of the HA term is indeed
333 significantly correlated with those of the VA and DH terms, suggesting the
334 relationship between the vertical motion (diabatic heating) and the relative flow.

335 The contribution of diabatic heating results mainly from $-\mathbf{q}_s \cdot \nabla_3 h_1$, where \mathbf{q}_s
336 is the symmetric component of the absolute vorticity, ∇_3 the three-dimensional
337 gradient operator, h_1 the wavenumber-one component of diabatic heating rate. Since
338 the absolute vorticity is dominated by the vertical component of relative vorticity and
339 diabatic heating rate reaches its maximum in the middle troposphere, it is conceivable
340 that the contribution of diabatic heating should cancel each other in the low and upper
341 troposphere. Figure 11 shows the contribution of diabatic heating at 700 hPa and 400
342 hPa. The correlation between 700 hPa and 400 hPa is -0.68 in the zonal direction and
343 -0.67 in the meridional direction.

344 **5. Trochoidal motion**

345 As shown in Fig. 5, the tropical cyclone motion exhibits considerable fluctuations.
346 In an instant, the steering can significantly deviate from the tropical cyclone motion.
347 At 60 h, for example, the zonal steering is -0.55 m s^{-1} , about one third of the zonal
348 motion of the tropical cyclone (-1.42 m s^{-1}); The meridional steering is 2.71 m s^{-1} ,
349 slower than the meridional motion of the tropical cyclone (3.05 m s^{-1}). The deviation
350 from the tropical cyclone motion is 13.5° in the direction and 18% in the magnitude.

351 Based on radar data and satellite images, many studies documented the oscillation
352 of a tropical cyclone track with respect to its mean motion vector (e.g., Jordan and
353 Stowell 1955; Lawrence and Mayfield 1977; Muramatsu 1986; Itano et al. 2002;
354 Hong and Chang 2005). The periods of track oscillations range from less than an hour
355 to a few days (Holland and Lander 1993). In this study, the small-scale oscillation
356 with amplitudes of that comparable to the eye size and periods of several hours is

357 referred to as the trochoidal motion of the tropical cyclone center. Willoughby (1988)
358 showed that a pair of rotating mass and sink source could lead to trochoidal motion
359 with periods ranging from 2-10 hours. Flatau and Stevens (1993) argued that
360 wavenumber-one instabilities in the outflow layer of tropical cyclones could cause
361 trochoidal motion. Nolan et al. (2001) found that the small-amplitude trochoidal
362 motion is associated with the instability of the wavenumber-one component of
363 tropical cyclone circulation due to the presence of the low-vorticity eye. The
364 instability in their three-dimensional simulation with a baroclinic vortex quickly led to
365 substantial inner-core vorticity redistribution and mixing, displacing the vortex center
366 that rotates around the vortex core. Our spectral analysis indicates two peaks of the
367 fluctuations of the tropical cyclone motion centered at 5 hours and 9 hours (Figure not
368 shown), suggesting that the trochoidal motion is simulated in our high-resolution
369 numerical simulation.

370 Figure 12 shows the oscillation of the tropical cyclone track with respect to the
371 9-hour running mean track for the periods 6-18 h and 59-70 h. We can see that the
372 displacement from the mean track is usually less than 6 km with a period of several
373 hours in this study. This displacement is less than the size of the tropical cyclone eye.
374 In general, the tropical cyclone center rotates cyclonically relative to the mean track
375 position, in agreement with previous observational and numerical studies (Lawrence
376 and Mayfield 1977; Muramatsu 1986; Itano et al. 2002; Willoughby 1988; Nolan et al.
377 2001). In association with the trochoidal motion of the tropical cyclone center, as
378 suggested by Nolan et al. (2001), substantial potential vorticity redistribution and

379 mixing can be observed in the inner core region (Fig. 13). During the period of 13-18
380 hours, the tropical cyclone eye generally looks like a triangle, but the orientation of
381 the triangle changes rapidly, suggesting the potential vorticity redistribution and
382 mixing in the eye.

383 The trochoidal motion is well indicated in the translation speed estimated with the
384 PVT approach. Figure 14a shows the fluctuations of tropical cyclone speed, the PVT
385 speed, and the difference between the tropical cyclone speed and the conventional
386 steering, in which the 9-hour running mean has been removed. We can see that the
387 fluctuations of tropical cyclone motion are well represented in the PVT speed.
388 Moreover, the consistence between the fluctuations of tropical cyclone motion and
389 those with the conventional steering removed suggests that the small-amplitude
390 oscillation of the tropical cyclone motion cannot be accounted for by the conventional
391 steering. Figure 14b further compares the time series of tropical cyclone motion
392 relative to the conventional steering with the time series of the contribution of the HA
393 term relative to the conventional steering. The two time series are correlated with a
394 coefficient of 0.60. We can see that the contribution of the HA term plays an
395 important role in the fluctuations. Since the non-steering effect can well account for
396 the fluctuations (Fig. 14a), Figure 14b suggests that the VA and DH tend to reduce the
397 magnitude of the fluctuations.

398 **6. Summary**

399 In this study, we addressed two fundamental questions regarding the steering
400 principle that has been widely applied to tropical cyclone forecast and research for

401 about a century (Fujiwara and Sekiguchi 1919; Bowie 1922). One is why the
402 conventional steering plays a dominant role in tropical cyclone motion and the other
403 is when tropical cyclone motion deviates considerably from the steering. The PVT
404 diagnosis approach proposed by Wu and Wang (2000) is used with the output from a
405 high-resolution numerical experiment. It is found that the PVT approach can well
406 estimate tropical cyclone motion, including the small-amplitude trochoidal motion
407 relative to the mean tropical cyclone track.

408 The effect of the conventional steering flow that is averaged over a certain radius
409 from the tropical cyclone center and a deep pressure layer (e.g., 850-300 hPa) actually
410 represents the combined contribution from both the advection of the symmetric
411 potential vorticity component by the asymmetric flow (HA1) and the advection of the
412 wavenumber-one potential vorticity component by the symmetric flow (HA2),
413 although the contribution of the HA1 term is literally the effect of steering (Wu and
414 Wang 2001a, 2001b). The conventional steering generally plays a dominant role in
415 tropical cyclone motion since the contributions from other processes are largely
416 cancelled out due to the coherent structure of tropical cyclone circulation.

417 The trochoidal motion of the tropical cyclone center is simulated in the numerical
418 experiment with amplitudes smaller than the eye radius and periods of several hours.
419 The tropical cyclone center rotates cyclonically around the mean track, in agreement
420 with previous observational and numerical studies (Lawrence and Mayfield 1977;
421 Muramatsu 1986; Itano et al. 2002; Willoughby 1988; Nolan et al. 2001). It is found
422 that the small-amplitude trochoidal motion cannot be accounted for by the effect of

423 the conventional steering although the contribution of the HA term plays an important
424 role in the fluctuations. In agreement with previous studies (Willoughby 1988; Nolan
425 et al. 2001), we suggest that the small-amplitude trochoidal motion results from the
426 asymmetric dynamics of the tropical cyclone inner core. It is also found that the
427 instantaneous speed of tropical cyclone motion can considerably deviate from the
428 conventional steering, while the latter better represents tropical cyclone motion when
429 averaged over a reasonable time period.

430 **Acknowledgements.** Many thanks go to Dr. Christopher W. Landsea of the National
431 Hurricane Center for providing us the early references on the steering principle. This
432 research was jointly supported by the National Basic Research Program of China
433 (2013CB430103, 2015CB452803), the National Natural Science Foundation of China
434 (Grant No. 41275093), and the project of the specially-appointed professorship of
435 Jiangsu Province. We appreciate Dr. C.-C. Wu and two anonymous reviewers for their
436 constructive comments.

437

438 **References:**

439 Bender, M. A., 1997: The effect of relative flow on the asymmetric structure in the
440 interior of hurricanes. *J. Atmos. Sci.*, **54**, 703–724.

441 Bowie, E. H., 1922: Formation and movement of West Indian hurricanes. *Mon. Wea.*
442 *Rev.*, **50**, 173-179.

443 Carr, L. E., and R. L. Elsberry, 1990: Observational evidence for predictions of
444 tropical cyclone propagation relative to steering. *J. Atmos. Sci.*, **47**, 542–546.

445 Chan, J. C. -L., F. M. F. Ko, and Y. M. Lei, 2002: Relationship between potential
446 vorticity tendency and tropical cyclone motion. *J. Atmos. Sci.*, **59**, 1317-1336.

447 Chan, J. C. -L., and W. M. Gray, 1982: Tropical cyclone motion and surrounding flow
448 relationship. *Mon. Wea. Rev.*, **110**, 1354-1374.

449 Chan, J. C. -L., 1984: An observational study of physical processes responsible for
450 tropical cyclone motion. *J. Atmos. Sci.*, **41**, 1036-1048.

451 Chan, J. C.-L., and R. T. Williams, 1987: Analytical and numerical studies of
452 beta-effect in tropical cyclone motion. Part I: Zero mean flow. *J. Atmos. Sci.*, **44**,
453 1257–1265.

454 Choi, Y., K.-S. Yun, K.-J. Ha, K.-Y. Kim, S.-J. Yoon, J.-C.-L. Chan, 2013: Effects of
455 Asymmetric SST Distribution on Straight-Moving Typhoon Ewiniar (2006) and
456 Recurving Typhoon Maemi (2003). *Mon. Wea. Rev.* **141**, 3950-3967.

457 Duchon, C. E., 1979: Lanczos filtering in one and two dimensions. *J. Appl. Meteor.*, **18**,
458 1016–1022.

459 Dudhia, J., 1989: Numerical study of convection observed during the winter monsoon
460 experiment using a mesoscale two-dimensional model. *J. Atmos. Sci.*, **46**,
461 3077-3107.

462 Flatau, M., W. H. Schubert, and D. E. Stevens, 1994: The role of baroclinic processes
463 in tropical cyclone motion: The influence of vertical tilt. *J. Atmos. Sci.*, **51**,
464 2589–2601.

465 Fiorino, M., and R. L. Elsberry, 1989: Some aspects of vortex structure related to
466 tropical cyclone motion. *J. Atmos. Sci.*, **46**, 975-990.

467 Fovell, R. G., K. L. Corbosiero, A. Seifert, and K.-N. Liou, 2010: Impact of
468 cloud-radiative processes on hurricane track, *Geophys. Res. Lett.*, **37**, L07808,
469 doi:10.1029/2010GL042691.

470 Frank, W., and E. A. Ritchie, 2001: Effects of vertical wind shear on the intensity and
471 structure of numerically simulated hurricanes. *Mon. Wea. Rev.*, **129**, 2249–2269.

472 Franklin, J. L., S. E. Feuer, J. Kaplan, and S. D. Aberson, 1996: Tropical cyclone
473 motion and surrounding flow relationship: Searching for beta gyres in Omega
474 dropwindsonde datasets. *Mon. Wea. Rev.*, **124**, 64–84.

475 Fujiwhara, S., and K. Sekiguchi, 1919: Estimated 300 m isobars and the weather of
476 Japan. *J. Meteor. Soc. Japan*, **38**, 254-259 (in Japanese).

477 Holland, G. J., 1983: Tropical cyclone motion: Environmental interaction plus a beta
478 effect. *J. Atmos. Sci.*, **40**, 328–342.

479 Houze, R.A., 2010: Clouds in tropical cyclones. *Mon. Wea. Rev.*, **138**, 293–344.

480 Hsu, L.-H., Hung-Chi Kuo, Robert G. Fovell, 2013: On the Geographic Asymmetry
481 of Typhoon Translation Speed across the Mountainous Island of Taiwan. *J.*
482 *Atmos. Sci.* **70**, 1006-1022.

483 Huang, Y.-H., M. T. Montgomery, and C.-C. Wu, 2012: Concentric eyewall
484 formation in Typhoon Sinlaku (2008) – Part II: Axisymmetric dynamical
485 processes. *J. Atmos. Sci.*, **69**, 662-674.

486 Itano, T., G. Naito, and M. Oda, 2002: Analysis of elliptical eye of Typhoon Herb
487 (T9609) (in Japanese with English abstract). *Sci. Eng. Rep. Natl. Def. Acad.*, **39**,
488 9–17.

489 Kain, J. S., and J. M. Fritch, 1993: Convective parameterization for mesoscale models:
490 the Kain-Fritch scheme. The representation of cumulus convection in numerical
491 models. *Meteorological Monographs*, **46**, 165-170.

492 Lawrence, M. B., and B. M. Mayfield, 1977: Satellite observations of trochoidal
493 motion during Hurricane Belle 1976. *Mon. Wea. Rev.*, **105**, 1458–1461.

494 Marks, F. D., Jr., R. A. Houze, Jr., and J. F. Gamache, 1992: Dual-aircraft
495 investigation of the inner core of Hurricane Norbert. Part I: Kinematic structure.
496 *J. Atmos. Sci.*, **49**, 919–942.

497 Mlawer, E. J., S. J. Taobman, P. D. Brown, M. J. Iacono, and S. A. Clough, 1997:
498 Radiative transfer for inhomogeneous atmosphere: RRTM, a validated
499 correlated-k model for the longwave. *J. Geophys. Res.*, **102**, 16663-16682.

500 Muramatsu, T., 1986: Trochoidal motion of the eye of Typhoon 8019. *J. Meteor. Soc.*
501 *Japan*, **64**, 259–272.

502 Noh, Y., W. G. Cheon, S.-Y. Hong, and S. Raasch, 2003: Improvement of the
503 K-profile model for the planetary boundary layer based on large eddy simulation
504 data. *Bound.-Layer Meteor.*, **107**, 401-427.

505 Neumann, C. J., 1993: Global overview. *Global Guide to Tropical Cyclone*
506 *Forecasting*, World Meteor. Org., 1.1–1.56.

507 Nolan, D. S., M. T. Montgomery, and L. D. Grasso, 2001: The wavenumber-one
508 instability and trochoidal motion of hurricane-like vortices. *J. Atmos. Sci.*, **58**,
509 3243–3270.

510 Riehl, H., and N. M. Burgner, 1950: Further studies on the movement and formation

511 of hurricanes and their forecasting. *Bull. Amer. Meteor. Soc.*, **31**, 244–253.

512 Riemer, M., 2016: Meso- β -scale environment for the stationary band complex of
513 vertically-sheared tropical cyclones. *Q. J. R. Meteorol. Soc.*, **142**, 2442–2451.

514 Simpson, R. H., 1946: On the movement of tropical cyclones. *Trans. Amer. Geophys.*
515 *Union*, **27**, 641-655.

516 Velden, C. S., and L. M. Leslie, 1991: The basic relationship between tropical cyclone
517 intensity and the depth of the environmental steering layer in the Australian
518 region. *Weather and Forecasting*, **6**, 244-253.

519 Wang, B., and X. Li, 1992: The beta drift of three-dimensional vortices: A numerical
520 study. *Mon. Wea. Rev.*, **120**, 579–593.

521 Wang, B., R. L. Elsberry, Y. Wang, and L. Wu, 1998: Dynamics of tropical cyclone
522 motion: A review. *Sci. Atmos. Sin.*, **22**, 1–12.

523 Wang, C.-C., Y.-H. Chen, H.-C. Kuo, S.-Y. Huang, 2013: Sensitivity of typhoon track
524 to asymmetric latent heating/rainfall induced by Taiwan topography: A numerical
525 study of Typhoon Fanapi (2010). *Journal of Geophysical Research: Atmospheres*
526 **118**, 3292-3308.

527 Wang, Y., and G. J. Holland, 1996a: The beta drift of baroclinic vortices. Part I:
528 Adiabatic vortices. *J. Atmos. Sci.*, **53**, 411–427.

529 Wang, Y., and G. J. Holland, 1996b: The beta drift of baroclinic vortices. Part
530 II: Diabatic vortices. *J. Atmos. Sci.*, **53**, 3737–3756.

531 Wang, Y., and G. J. Holland, 1996c: Tropical cyclone motion and evolution in vertical
532 shear. *J. Atmos. Sci.*, **53**, 3313–3332.

533 Willoughby, H., 1988: Linear motion of a shallow-water, barotropic vortex. *J. Atmos.*
534 *Sci.*, **45**, 1906–1928.

535 Wu, C.-C., and K. A. Emanuel, 1993: Interaction of a baroclinic vortex with
536 background shear: Application to hurricane movement. *J. Atmos. Sci.*, **50**, 62–76.

537 Wu, C.-C., and K. A. Emanuel, 1995a: Potential vorticity diagnostics of hurricane
538 movement. Part I: A case study of Hurricane Bob (1991). *Mon. Wea. Rev.*, **123**,
539 69–92.

540 Wu, C.-C., and K. A. Emanuel, 1995b: Potential vorticity diagnostics of hurricane
541 movement. Part II: Tropical Storm Ana (1991) and Hurricane Andrew (1992).
542 *Mon. Wea. Rev.*, **123**, 93–109.

543 Wu, C.-C., Y.-H. Huang, and G.-Y. Lien, 2012: Concentric eyewall formation in
544 Typhoon Sinlaku (2008) – Part I: Assimilation of T-PARC data based on the
545 Ensemble Kalman Filter (EnKF). *Mon. Wea. Rev.*, **140**, 506-527.

546 Wu, L., and B. Wang, 2000: A potential vorticity tendency diagnostic approach for
547 tropical cyclone motion. *Mon. Wea. Rev.*, **128**, 1899-1911.

548 Wu, L., and B. Wang, 2001a: Movement and vertical coupling of adiabatic baroclinic
549 tropical cyclones. *J. Atmos. Sci.*, **58**, 1801-1814.

550 Wu, L., and B. Wang, 2001b: Effects of convective heating on movement and vertical
551 coupling of tropical cyclones: A numerical study. *J. Atmos. Sci.*, **58**, 3639-3649.

552 Wu, L., J. Liang, and C.-C. Wu, 2011a: Monsoonal Influence on Typhoon Morakot
553 (2009). Part I: Observational analysis. *J. Atmos. Sci.*, 2208–2221.

554 Wu, L., H. Zong, and J. Liang, 2011b: Observational analysis of sudden tropical

555 cyclone track changes in the vicinity of the East China Sea. *J. Atmos. Sci.*, **68**,

556 3012–3031.

557 Wu, L., S. A. Braun, J. Halverson, and G. Heymsfield, 2006: A numerical study of

558 Hurricane Erin (2001). Part I: Model verification and storm evolution. *J. Atmos.*

559 *Sci.*, **63**, 65–86.

560 Yu, H., W. Huang, Y. H. Duan, J. C. L. Chan, P. Y. Chen, R. L. Yu. (2007) A

561 simulation study on pre-landfall erratic track of typhoon Haitang (2005).

562 *Meteorology and Atmospheric Physics*, **97**, 189-206.

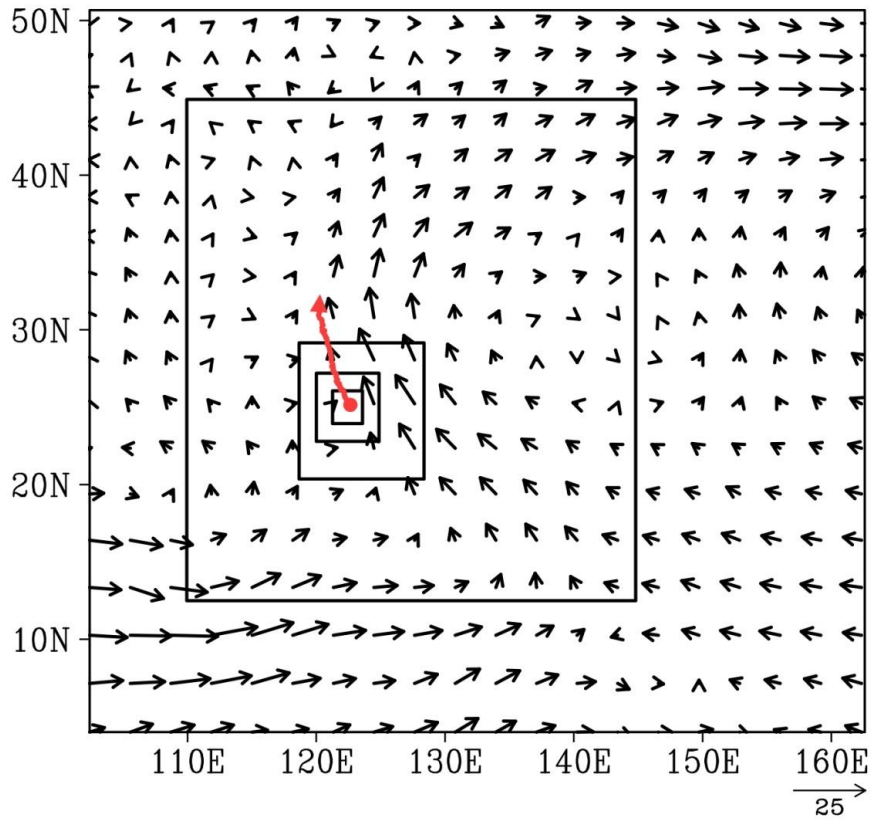
563

564

565

566

567

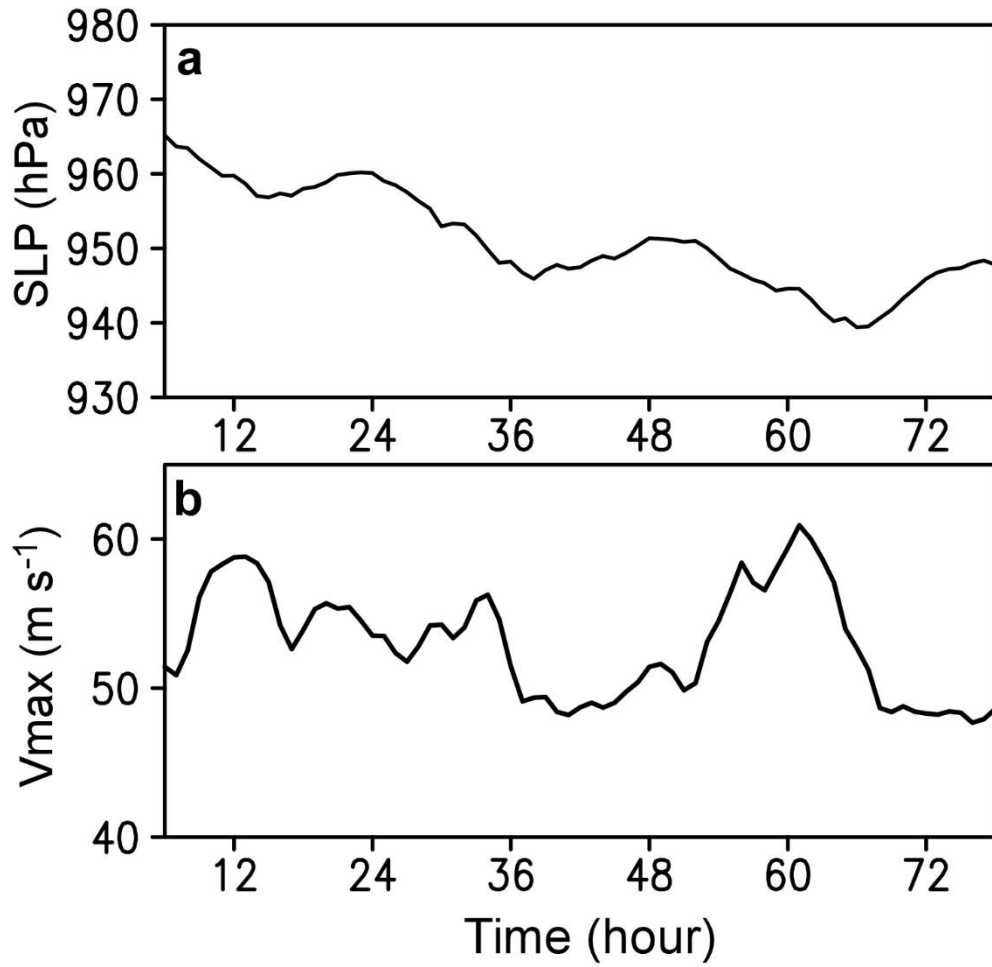


568

569 Figure 1 Model domains of the numerical experiment with the three innermost

570 domains moving with the storm, the initial 850-hPa wind (m s^{-1}) field (vectors), and

571 the simulated tropical cyclone track (red)

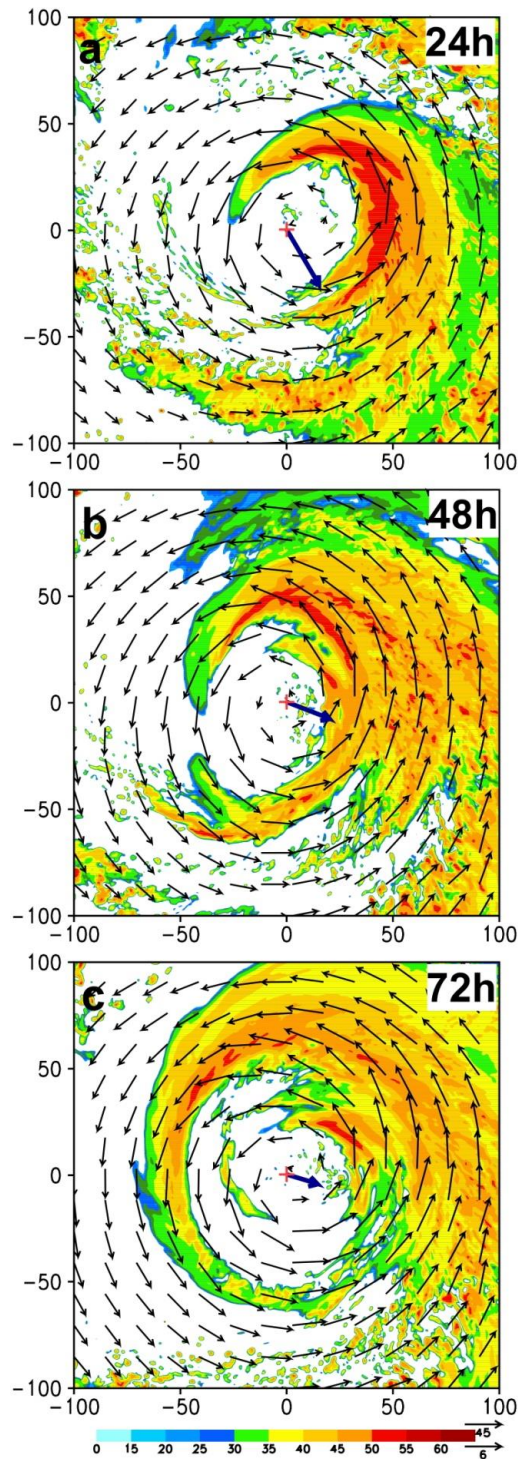


572

573 Figure 2 Time series of tropical cyclone intensity: a) sea level minimum pressure

574 (hPa); b) maximum wind speed at 10 m (m s⁻¹).

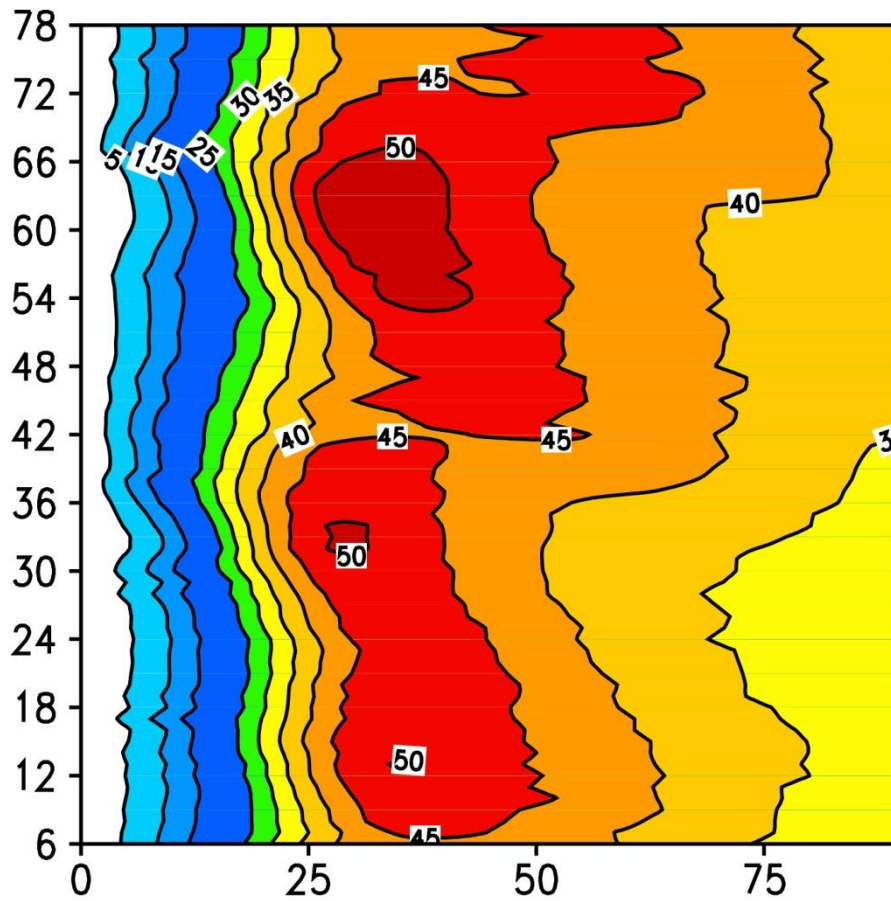
575



576

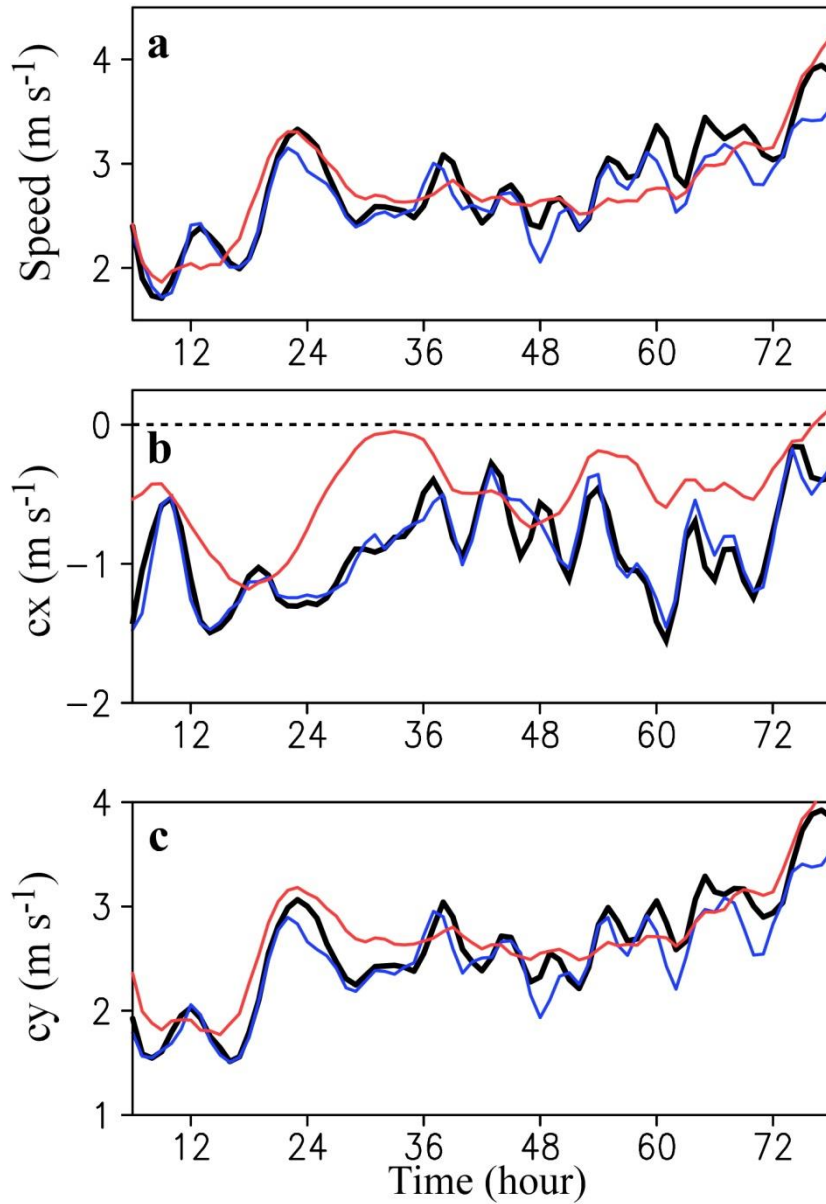
577 Figure 3 Simulated wind (vectors, m s^{-1}), radar reflectivity (shading, dBz) fields at
 578 700 hPa, and the vertical wind shear (bold arrows in the center) between 200 hPa and
 579 850 hPa after (a) 24-h, (b) 48-h, and (c) 72-h integration. The x and y axes indicate
 580 the distance (km) relative to the storm center. The upper (lower) scale vector at the
 581 right lower corner is for the 700-hPa wind (vertical wind shear).

582



583

584 Figure 4 Evolution of the simulated azimuthal mean component (m s^{-1}) of the 700-hPa
 585 wind in the 9-km domain. The x-axis and y-axis indicate the distance (km) from the
 586 storm center and the integration time (hours).



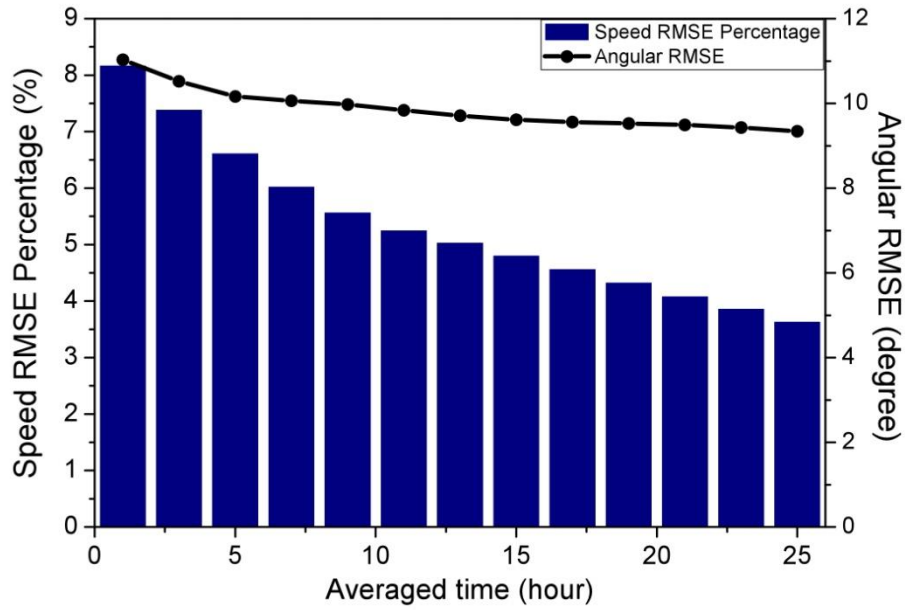
587

588 Figure 5 Time series of tropical cyclone speed (thick black), PVT speed (blue) and

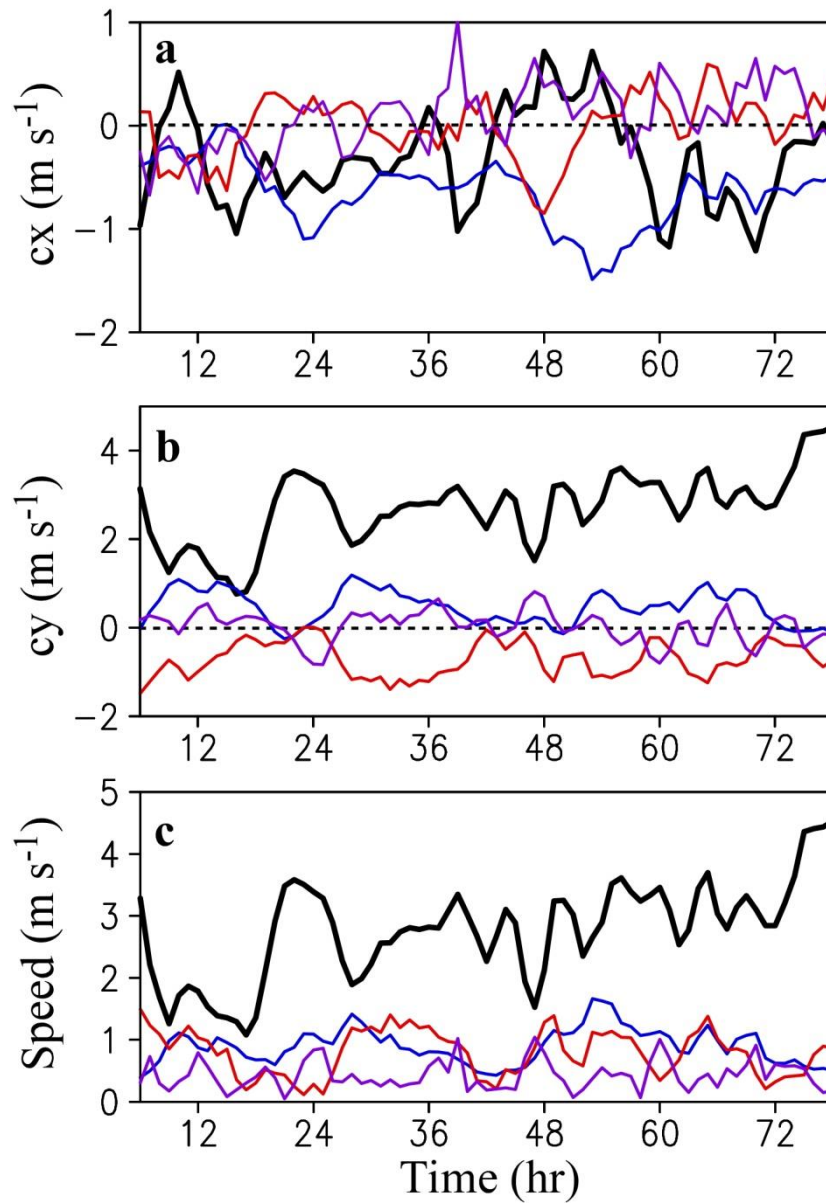
589 conventional steering (red): a) magnitude, b) zonal component, and c) meridional

590 component

591



592
 593 Figure 6 Changes of the RMSEs of the speed (blue boxes, %) and direction (black
 594 dots, °) of the conventional steering averaged over various time periods



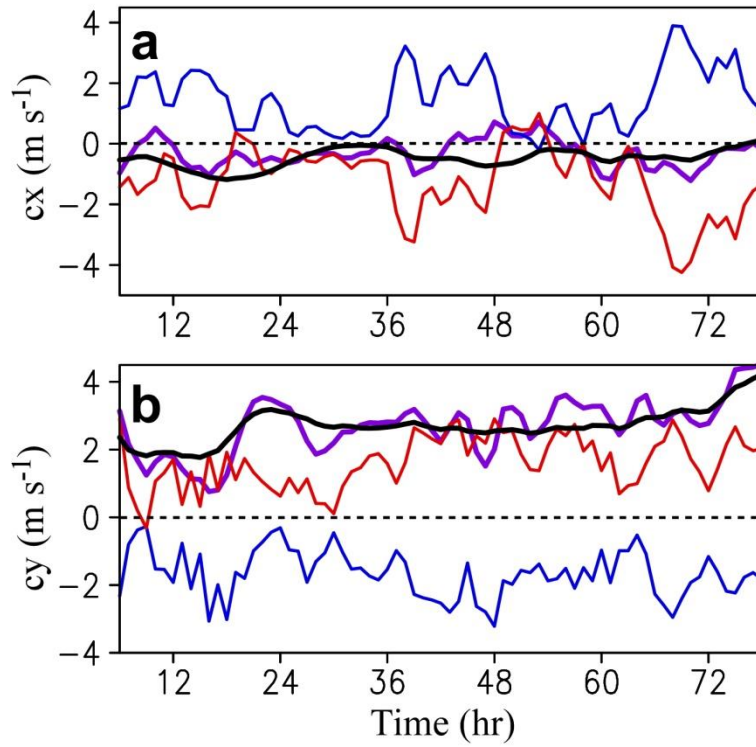
595

596 Figure 7 Contributions of the horizontal advection (HA, black), vertical advection

597 (VA, blue), diabatic heating (DH, red) and friction (FR, purple) terms in the PVT

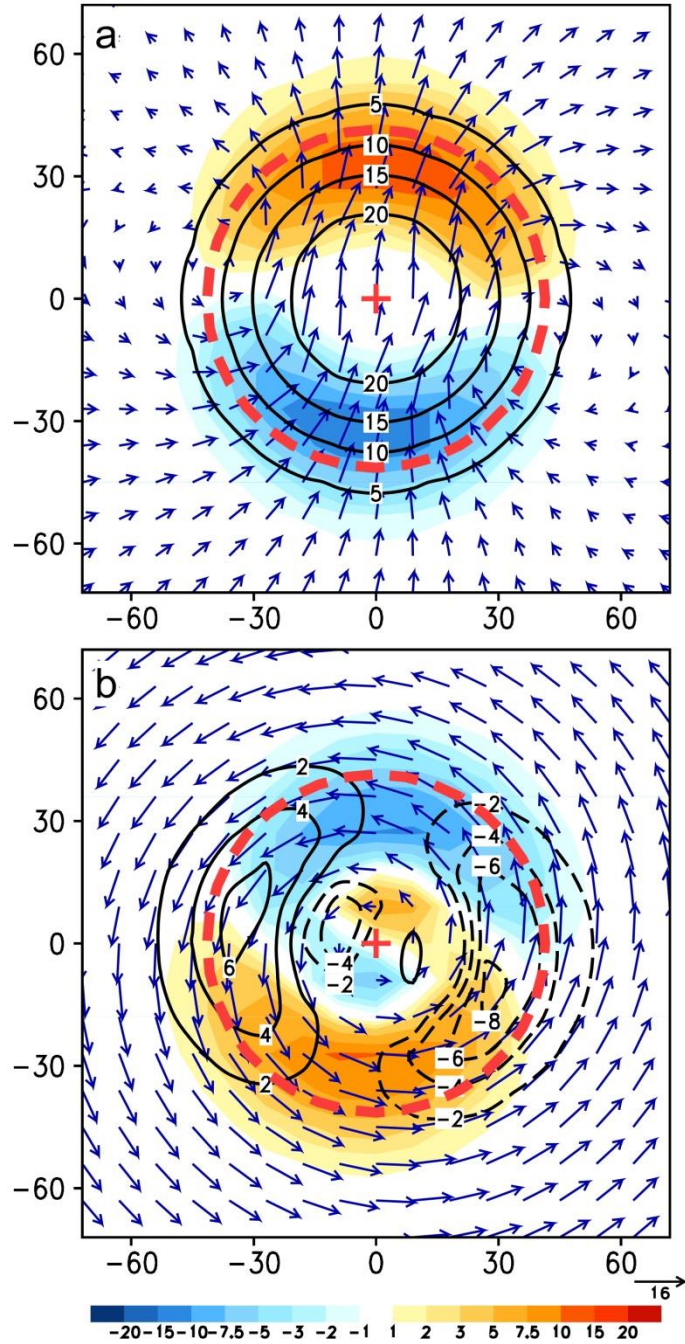
598 equation to tropical cyclone motion: a) zonal component, b) meridional component,

599 and c) magnitude



600

601 Figure 8 Time series of the conventional steering (thick black) and the contributions
 602 of the HA (thick purple) and the HA1 (red) and HA2 (blue) terms: a) zonal
 603 component, b) meridional component. Note that the conventional steering is deducted
 604 from the contribution of the HA1 term.



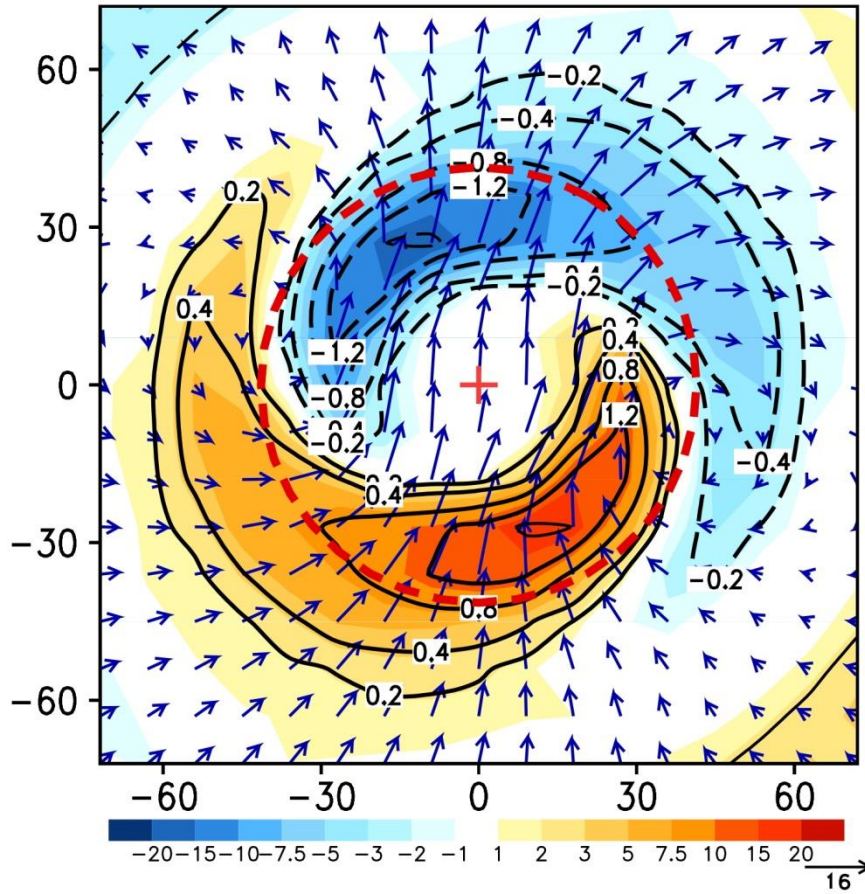
605

606 Figure 9 (a) HA1 (shaded, $10^{-10} \text{ m}^2 \text{ s}^{-2} \text{ K kg}^{-1}$) and (b) HA2 (shaded, $10^{-10} \text{ m}^2 \text{ s}^{-2} \text{ K}$

607 kg^{-1}) with the wavenumber-one and symmetric components of potential vorticity

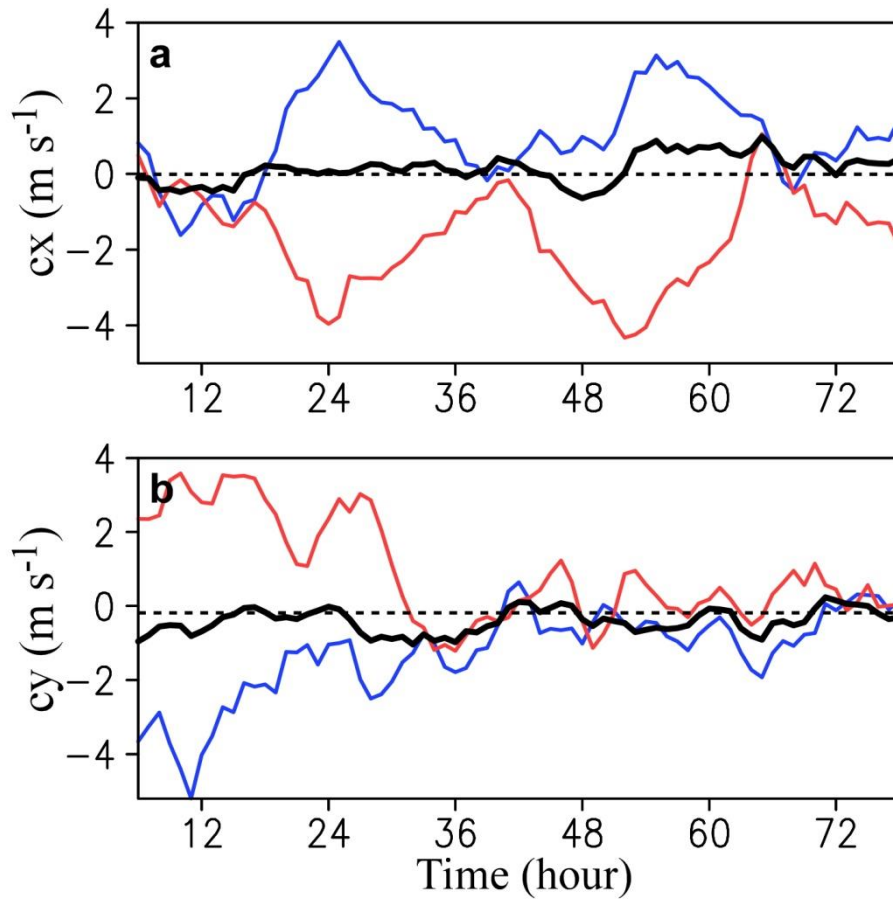
608 (contours, $10^{-6} \text{ m}^2 \text{ s}^{-1} \text{ K kg}^{-1}$) and winds (vectors, m s^{-1}) at 700 hPa after 18 hours of

609 integration. The dashed circle indicates the radius of maximum wind.



610

611 Figure 10 The wavenumber-one components of the 500-hPa vertical motion (contours,
 612 m s^{-1}), 700-hPa winds relative to the tropical cyclone motion (vectors, m s^{-1}), and
 613 500-hPa heating rate (shaded, 10^{-4} K s^{-1}) after 18 hours of integration. The dashed
 614 circle indicates the radius of maximum wind.

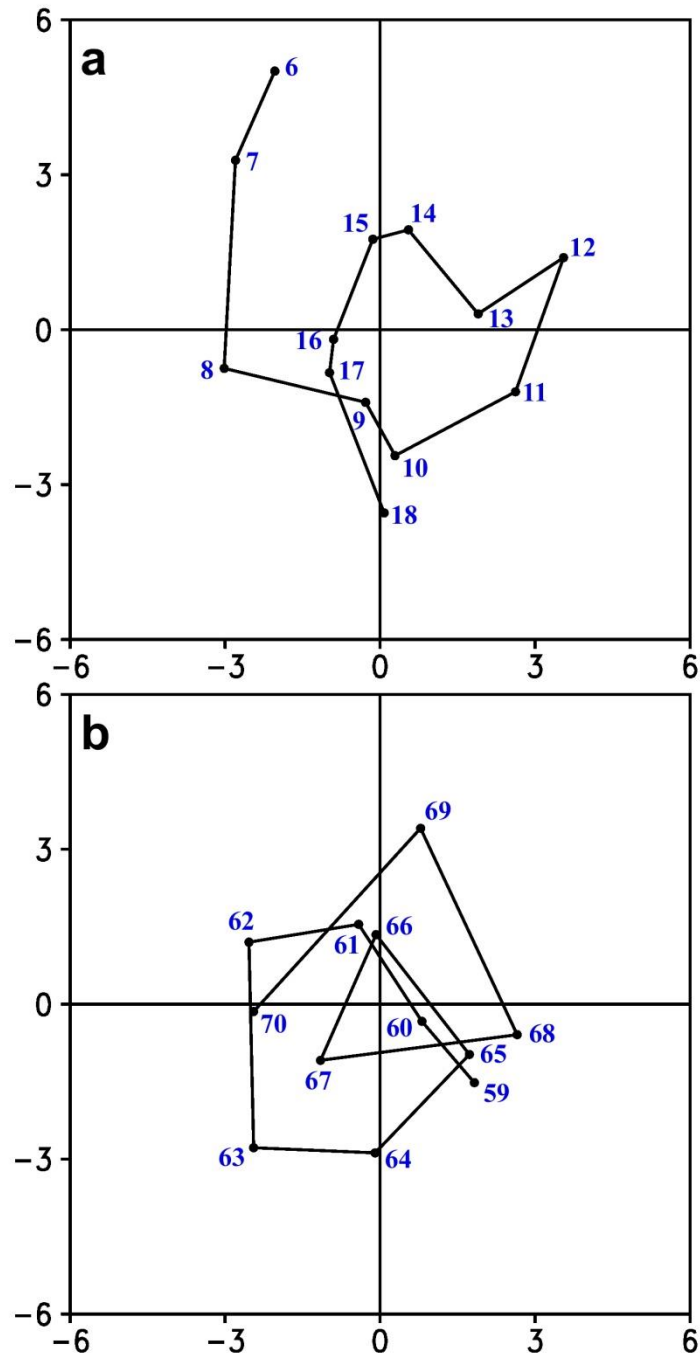


615

616 Figure 11 Time series of the contributions of diabatic heating at 700 hPa (blue) and

617 400 hPa (red) and the contribution of diabatic heating (thick black) averaged over the

618 layer between 300 hPa and 850 hPa



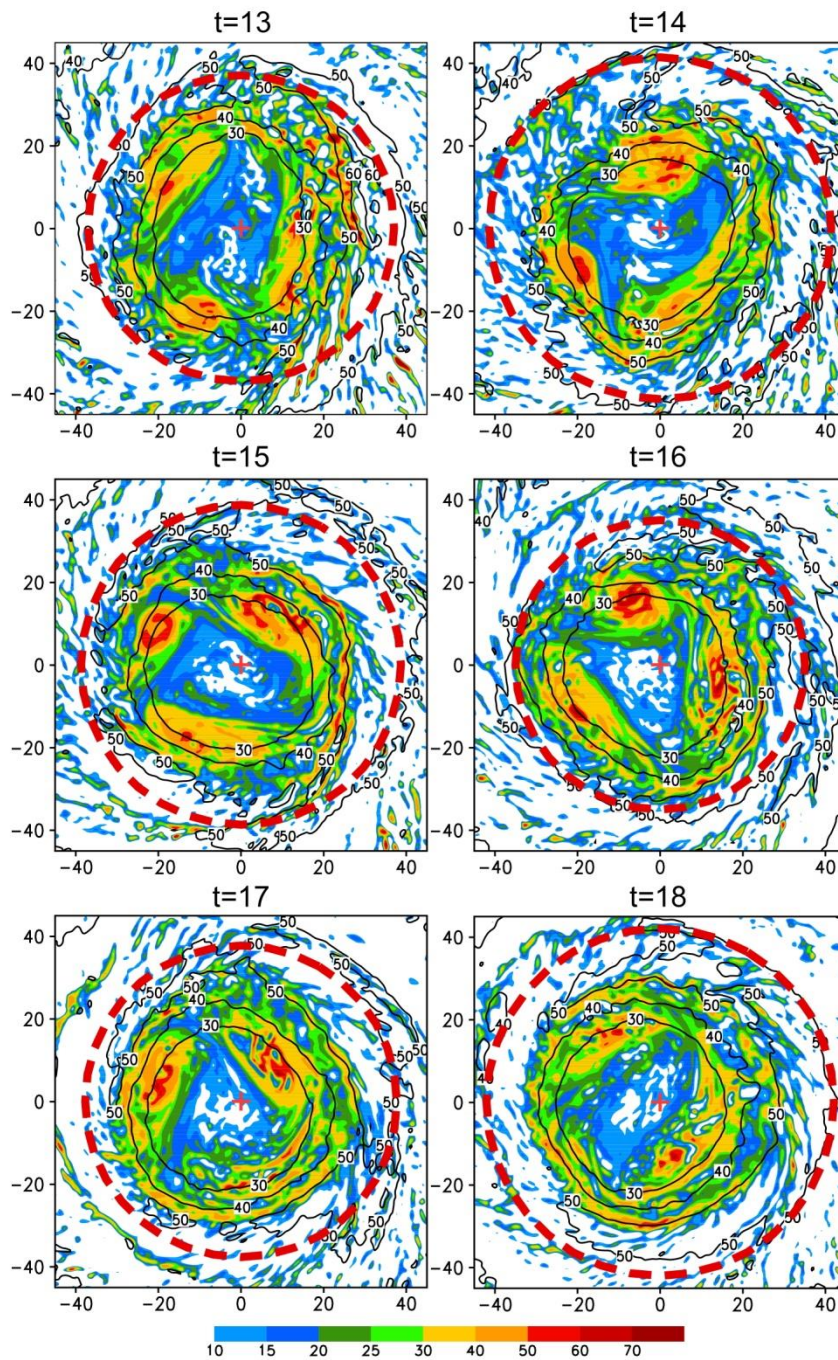
619

620 Figure 12 Small-amplitude oscillation of the tropical cyclone track with respect to the

621 9-hour running mean track: a) 6-18 h and b) 59-69 h. The x and y axes indicate the

622 distance (km) relative to the 9-hour running mean track.

623



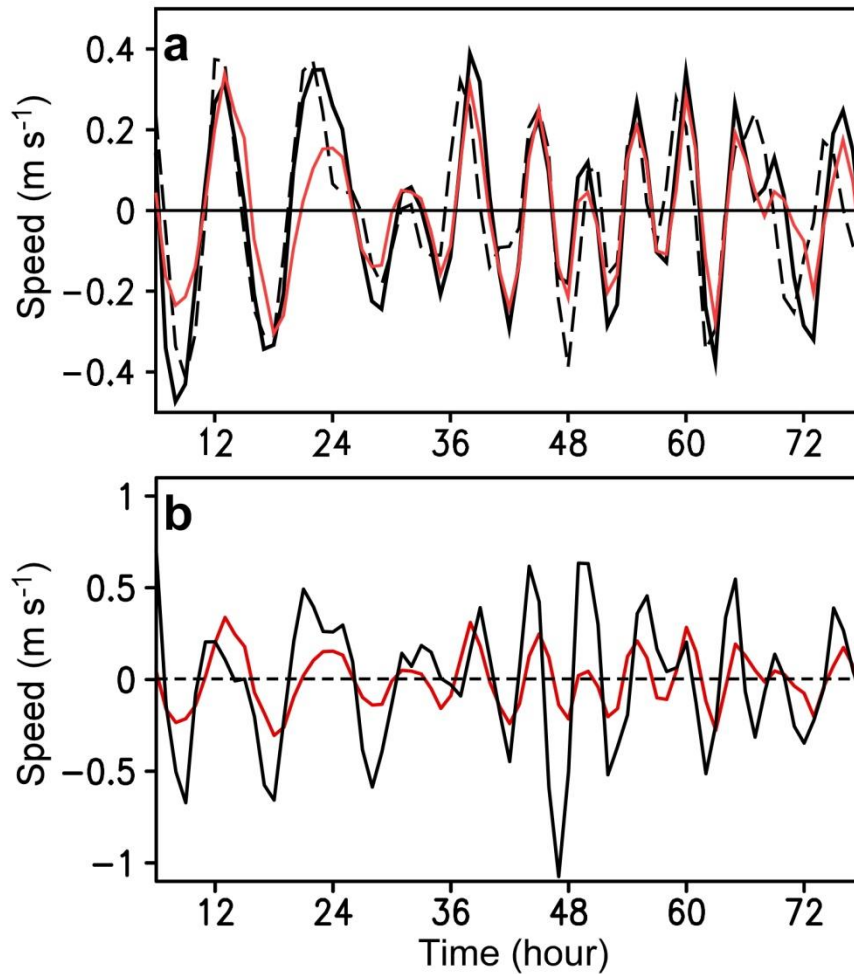
624

625 Figure 13 Distribution of potential vorticity (shaded, $10^{-6} \text{ m}^2 \text{ s}^{-1} \text{ K kg}^{-1}$) and
 626 magnitude of wind (contour, m s^{-1}) within inner-core region during 13-18 h at 700 hPa.

627 The dashed circle shows the radius of maximum wind with the tropical cyclone center
 628 indicating with crosses.

629

630



631

632

633 Figure 14 Fluctuations (deviation from the 9-hour running mean) of (a) the tropical
 634 cyclone speed (black solid), the PVT speed (black dashed) and the difference between
 635 the tropical cyclone speed and the conventional steering (red solid), and (b) the
 636 difference between the tropical cyclone speed and the conventional steering (red
 637 solid), and the difference between the contribution of the HA term and the
 638 conventional steering (black).

639

640